



Contents lists available at ScienceDirect

Materials Research Bulletin

journal homepage: www.elsevier.com/locate/matresbuGrowth and NO₂ sensing properties of Cs₂SnI₆ thin filmPham Tien Hung^{a,1}, Phung Dinh Hoat^{b,1}, Tien-Anh Nguyen^a, Pham Van Thin^a, Vu Xuan Hien^c,
Hyo-Jun Lim^b, Sangwook Lee^{b,d}, Joon-Hyung Lee^{b,d}, Young-Woo Heo^{b,d,*,#}^a Department of Physics, Le Quy Don Technical University, No. 236 Hoang Quoc Viet Street, Cau Giay District, Hanoi, Vietnam^b School of Materials Science and Engineering, Kyungpook National University (KNU), Daegu 41566, South Korea^c School of Engineering Physics, Hanoi University of Science and Technology, No. 01 Dai Co Viet Street, Hanoi, Vietnam^d KNU Advanced Material Research Institute, Kyungpook National University, Daegu 41566, South Korea

ARTICLE INFO

Keywords:

Cs₂SnI₆
Halide perovskite
CVD method
NO₂
gas sensors

ABSTRACT

In this study, Cs₂SnI₆ thin film was synthesized on a glass substrate through a two-step process using the chemical vapor deposition (CVD) method and was subsequently used as a NO₂ gas sensor. First, the CsI spheres with an average diameter of 360 nm were fabricated on the glass substrate using a CVD system at 240 °C. Second, Cs₂SnI₆ film was formed through the reaction of CsI spheres with SnI₄ vapor at 200 °C for 1 h. Finally, the as-synthesized Cs₂SnI₆ thin film based gas sensor was then fabricated to explore its potential applications. The results indicated that the device showed good selectivity, stability, and detection for NO₂ with low concentration at room temperature. In addition, the effect of humidity on NO₂-sensing performance of the device was further studied. Furthermore, the NO₂ sensing mechanism of the Cs₂SnI₆ thin film was discussed. Hence, this study helps understand the gas sensing mechanism of halide perovskite Cs₂SnI₆ and the room temperature development of NO₂ gas sensors.

1. Introduction

Recently, organic-inorganic lead halide perovskites have been extensively studied recently due to their unique properties for applications in several fields such as light-emitting diodes [1], solar cells [2–4], lasers [5], and photodetectors [6]. For gas sensor applications, sensors based on these materials are also interesting to study. For example, Yuan et al. synthesized CH₃NH₃PbI_{3-x} film via a solution-processing approach and reported that the CH₃NH₃PbI_{3-x} device can detect NO₂ and acetone vapor gas at room temperature [7]. Bao et al. fabricated MAPbI₃ film and investigated the conductivity change of the film induced by NH₃ [8]. They found that the current through the film was greatly improved within seconds of ammonia (NH₃) introduction. This material was also investigated the O₂ [9] and NO₂ [10] sensing properties. Zhu et al. have successfully synthesized a novel halide perovskite (C₄H₉NH₃)₂PbI₄ for the detection of p-xylene at low temperature [11]. The gas sensing properties based on hybrid lead mixed halide perovskite were also investigated [12]. Also, several studies reported that sensors based on

organic-inorganic lead halide perovskites operate at room temperature [7–10,12,13] or low temperature [11], which is extremely useful for gas sensor applications. The drawbacks of organic-inorganic lead halide perovskites are their instability under atmospheric conditions and the toxic lead component, which hinders their application as gas sensors [8, 14]. Various attempts have been made to address these issues by decorating graphene with halide perovskite [15, 16] or altering the compositions of halide perovskite to replace toxic lead with safer materials and improve their stability [17–19]. Among them, the tin (Sn)-based halide perovskites are of particular interest [20]. Qiu et al. synthesized air-stable Cs₂SnI₆ from the oxidative conversion of unstable B-γ-CsSnI₃ [21]. Chen et al. fabricated MASnI₃-SnO₂ composites with p-n junctions for rapid NO₂ sensing response properties at room temperature [22]. They discovered that testing 5 ppm NO₂ for 35 days gave the sensor long-term. By 2020, our team has discovered that MASnI₃ membranes can detect NO₂ with ppb concentration at room temperature [23].

In this study, we report a Cs₂SnI₆-based chemical gas sensor, which can selectively detect NO₂ at room temperature with ppm concentration

* Corresponding author at: School of Materials Science and Engineering, Kyungpook National University, Daegu 41566, South Korea.

E-mail address: ywheo@knu.ac.kr (Y.-W. Heo).¹ Equal authorship[§] Kyungpook National University (KNU), 80 Daehakro, Buk-gu, Daegu 41566, Korea[#] Post address: E8-215, 80 Daehakro, Buk-gu, Daegu 41,566, Korea<https://doi.org/10.1016/j.materresbull.2021.111628>

Received 24 July 2021; Received in revised form 18 October 2021; Accepted 2 November 2021

Available online 6 November 2021

0025-5408/© 2021 Elsevier Ltd. All rights reserved.

without light illumination. The detection limit for NO₂ gas was determined to be 3 ppm.

2. Materials and methods

2.1. The synthesis of the Cs₂SnI₆ thin film

A two-step procedure was used to synthesize the Cs₂SnI₆ film on a glass substrate with Au interdigitated electrodes using a CVD system. First, CsI spheres were fabricated, and subsequently, Cs₂SnI₆ thin film was synthesized via the conversion process of CsI film from SnI₄ vapor. Fig. 1 depicts the experimental setup. The glass substrate (10×20 mm²) was successively ultrasonicated for 10 min in acetone, ethanol, and distilled, then treated with UV – ozone for 10 min. The width and gap of the finger electrode are both 200 μm. In the first step, the CsI powder source (Sigma-Aldrich 99.99%) was placed into the middle of a quartz tube in an alumina boat. The glass substrate was placed downstream inside a quartz tube with a growth temperature of 240 °C as shown in Fig. 1a. A slight amount of N₂ gas was introduced into the quartz tube to maintain the pressure at 0.1 Torr. For the evaporation of the CsI source, the electric furnace was heated to 350 °C at a rate of 5 °C/min and kept at that temperature for 15 min. At the end of the first step, the white film CsI substrate was obtained.

In the second step, the as-synthesized sample was directly inserted into the center of the quartz tube while the SnI₄ powder source was placed upstream. The furnace temperature was then raised from room temperature to 200 °C for 20 min before being maintained at 200 °C for 60 min. The evaporation temperature of the SnI₄ source was 80 °C (Fig. 1b). The pressure inside the tube was maintained at 0.15 Torr during the conversion process. Finally, the furnace was allowed to cool naturally to ambient temperature and a black film of Cs₂SnI₆ was obtained.

2.2. Sensor fabrication and gas sensing measurement

The Cs₂SnI₆ film was deposited into glass substrates with an Au electrode (gap of 200 μm and line thickness of 200 μm) for gas sensor applications utilizing the aforesaid procedure. The structure of the electrode and the optical microscopy image of a sensor with Cs₂SnI₆ are

presented in Fig. S1.

A dynamic gas-testing system in a light-shielding chamber was used to explain the Cs₂SnI₆ device's gas sensitivity. The gas flowed directly onto the Cs₂SnI₆ device surface during the gas testing process, with a total gas flow rate of 200 sccm and dry air as the carrier gas. The gas sensing measurement was carried out at room temperature (25 °C) using a Keithley 4200-SCS system. The sensitive response (*S*) of the Cs₂SnI₆ device is defined as $S = 100\% \times \frac{|R_g - R_a|}{R_a}$, where *R*_a denotes the device's initial resistance in air and *R*_g denotes the device's resistance in the target gas. The times taken by the sensor to achieve 90% of the total resistance change during the adsorption and desorption processes are defined as the response and recovery times, respectively.

2.3. Characterization

Field emission electron microscopy (FE-SEM - JSM-6701F) was used to analyze the morphologies of as-prepared samples at a 10 kV accelerating voltage. The phase composition, crystallinity, and chemical composition of each sample were determined via X-ray diffraction (XRD; CuKα radiation, λ = 1.54178 Å) at potential and current of 40 kV and 30 mA, respectively. The UV–visible of the sample was measured using a spectrophotometer (Cary 5000 UV–vis-NIR). X-ray spectroscopy was also used to study the chemical composition of the sample surface (XPS, Quatera SXM).

3. Results and discussion

3.1. Morphology and structure

Fig. 2a, b shows XRD patterns of CsI spheres and Cs₂SnI₆ film on the glass substrate after the 1st and 2nd steps, respectively. Fig. 2a shows that all diffraction peaks in the XRD patterns can be indexed to the CsI cubic structure CsI (JCPDS card No. 01–089–4257). Fig. 2b shows the XRD pattern of the Cs₂SnI₆ film. The strong peaks at 2θ of 13.10°, 26.50°, 30.68°, and 43.94°, correspond to the (111), (222), (400), and (440) reflections of the Cs₂SnI₆ cubic structure (JCPDS card No. 01–073–0330). In addition, the peak corresponding to the Au electrode was also observed at 2θ of 38.56° (Fig. 2a, b). Besides the Au peak, there were no peaks corresponding to any other impurities were found,

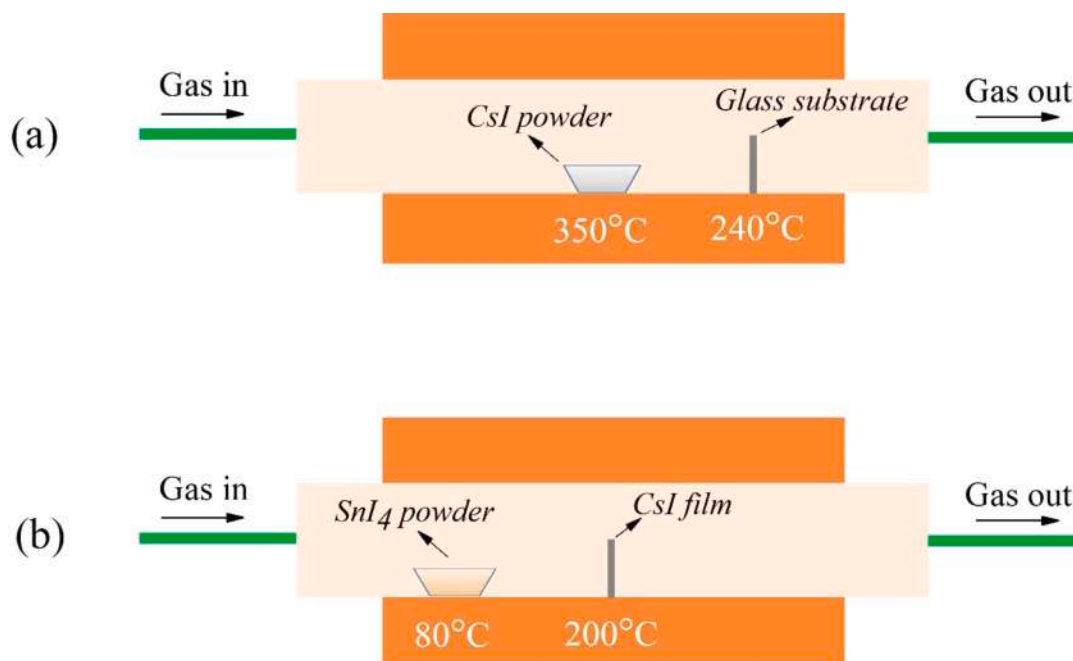


Fig. 1. Schematic diagram of CVD system: (a) fabrication of CsI spheres; (b) fabrication of Cs₂SnI₆ film.

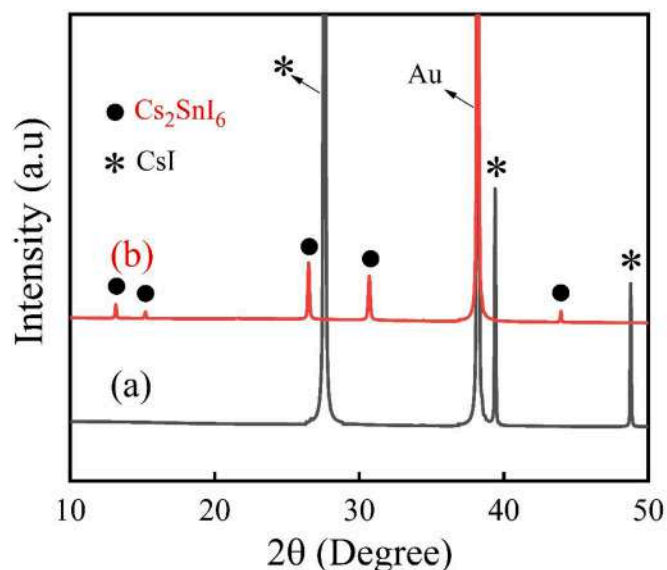


Fig. 2. XRD spectra of (a) CsI spheres after step 1; and (b) Cs_2SnI_6 film after step 2.

indicating that high-purity film was formed after each step process. CsI spheres with diameters of 350–450 nm were synthesized after the first step (Fig. 3). Fig. 3b shows the CsI film with a thickness of approximately 450 nm. Many spaces between the CsI spheres exist, which may help to promote the diffusion process of SnI_4 vapor in the second step. Fig. 3c shows the rough surface of the as-synthesized Cs_2SnI_6 film is composed of particles that are tightly packed together, thereby resulting in a continuous 1- μm -thick film (Fig. 3d).

The absorbance and the variation of $(abs. hv)^2$ with photon energy hv were exhibited in Fig. 4a and Fig. 4b, respectively. Assuming a direct band gap for Cs_2SnI_6 , the optical band gap calculated for Cs_2SnI_6 film is

1.61 eV, which is consistent with previous studies [21, 24, 25].

The composition and chemical states of the Cs_2SnI_6 film were investigated by XPS (Fig. 5). Only the energy peaks of Sn, Cs, and I appeared in the survey XPS spectra (Fig. 5a), indicating that the Cs_2SnI_6 film has extremely high purity. Fig. 5b shows the high-resolution XPS spectrum of Sn 3d Two spin-orbit peaks located at 486.92 and 495.44 eV demonstrate the presence of tin ions in the form of Sn^{4+} [26] rather than Sn^{2+} and Sn^0 [27]. Fig. 5c shows the high-resolution XPS spectrum of Cs 3d The binding energy of 724.58 and 738.53 eV can be attributed to Cs^{+1} 3d_{5/2} and Cs^{+1} 3d_{3/2}, respectively. This result is consistent with that in a previous report [28]. Fig. 5d shows the curve-fitting analysis of I 3d spectra, indicating a perfect fit into I^{1-} 3d_{5/2} (619.27 eV) and I^{1-} 3d_{3/2} (630.27 eV), with a spin energy separation of 11.5 eV, which agrees with previous study [28].

To evaluate the gas sensing properties of the Cs_2SnI_6 film, several harmful gasses i.e., NO_2 , CO_2 , CH_4 , H_2S , SO_2 , and C_3H_8 , were used as test gasses at room temperature without light illumination using a dynamic gas-testing system (Fig. S2). Fig. 6a displays the dynamic response of Cs_2SnI_6 film with exposure to 20 ppm of NO_2 operating at 25 °C. The behavior of Cs_2SnI_6 film represents the n-type metal oxide semiconductor properties. The resistance of the Cs_2SnI_6 film increased dramatically upon exposure to NO_2 gas caused by the charge transfer chemisorption on the Cs_2SnI_6 perovskite between NO_2 and oxygen adatoms. The original resistance of the device can be recovered after removing the NO_2 molecules by flowing dry air at room temperature (Fig. 6a). This sensor's response and recovery times at room temperature of 20 ppm NO_2 are 247 and 818 s, respectively. These response times may be improved by using a light irradiation, metal decorating/doping or applying some nanostructures/heterostructures. Fig. 6b shows the gas response of Cs_2SnI_6 film to various harmful gasses at room temperature. It can be clearly seen that the Cs_2SnI_6 is sensitive toward NO_2 but there are no changes in the gas response of the film to other gasses (e.g., NH_3 , SO_2 , CO_2 , CH_4 , and C_3H_8). It indicates that the Cs_2SnI_6 film was highly selective for NO_2 compared to other gasses. Fig. 7a shows the sensor resistance changes to various NO_2 concentrations at room temperature.

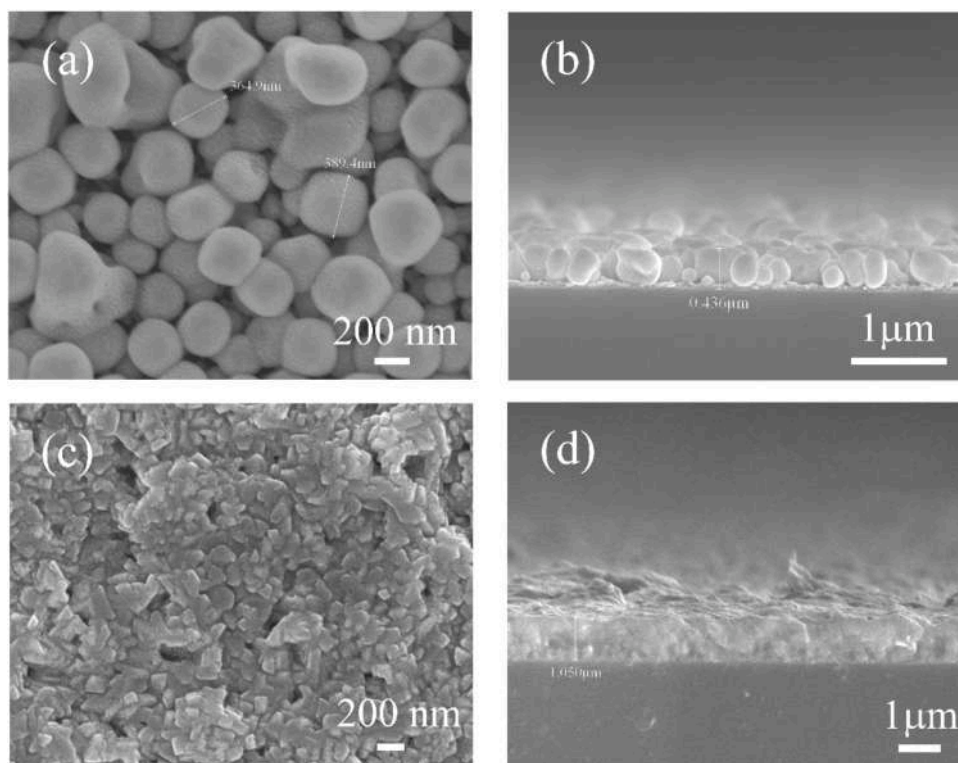


Fig. 3. Top-view and cross-sectional FE-SEM images of (a- and b) CsI spheres; and (c- and d) Cs_2SnI_6 film, respectively.

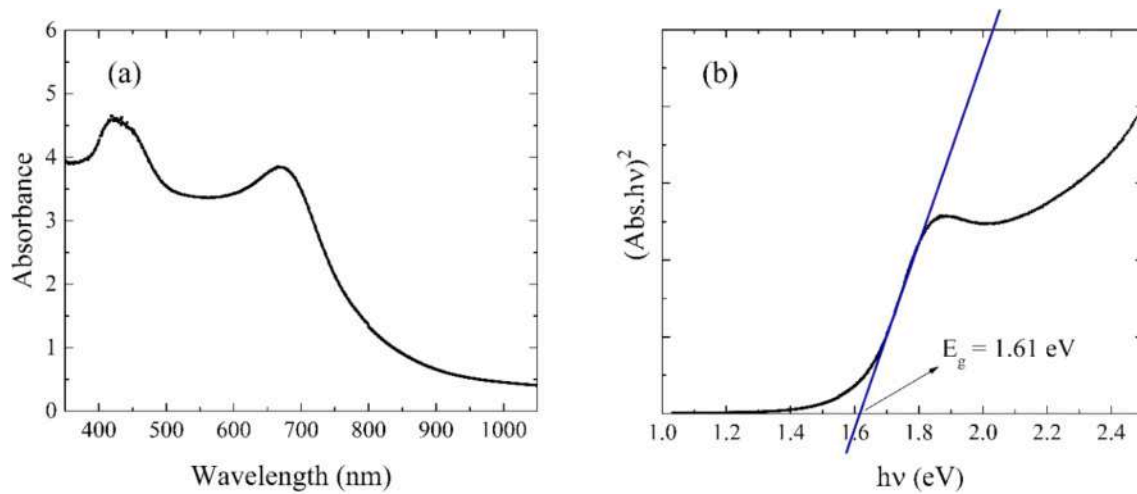


Fig. 4. Optical characterization of the Cs_2SnI_6 thin film: (a) absorbance of 1- μm -thick Cs_2SnI_6 film grown by the CVD method and (b) variation of $(\text{abs.}h\nu)^2$ with photon energy ($h\nu$).

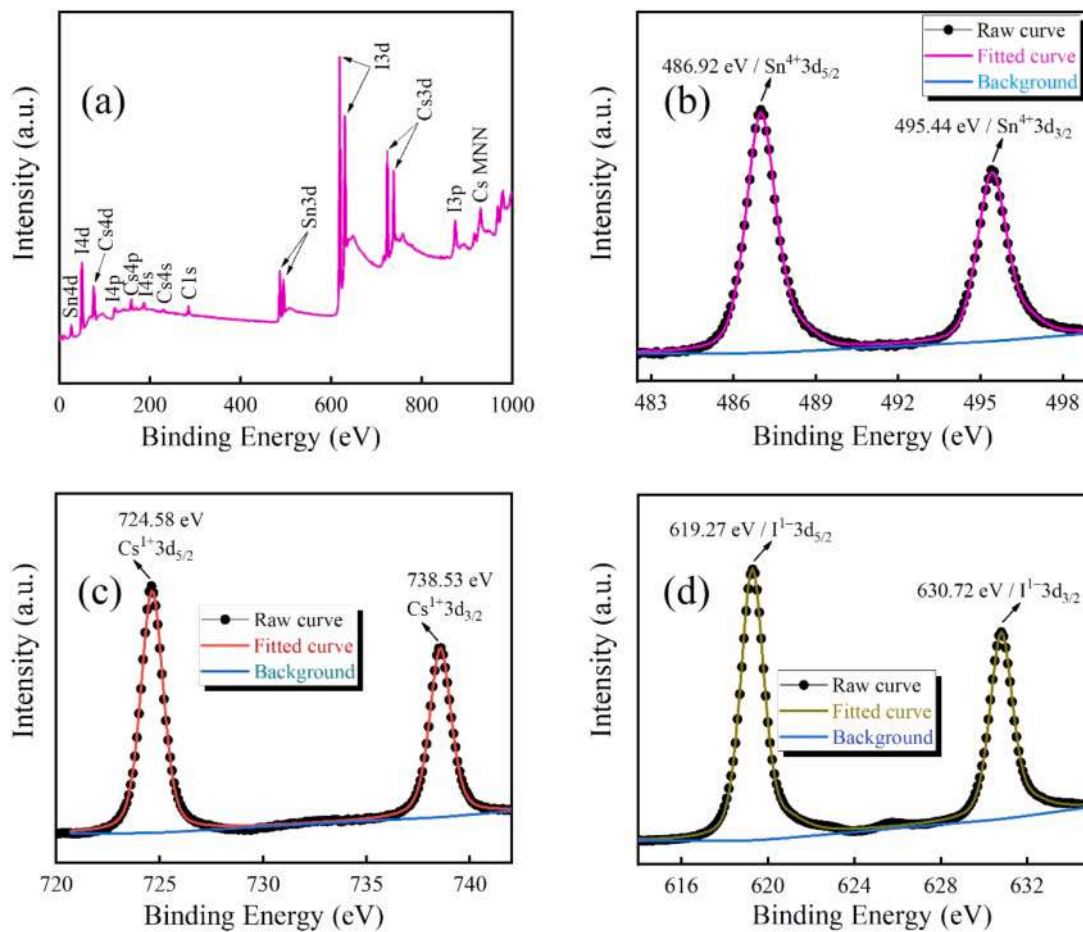


Fig. 5. (a) Survey X-ray photoelectron spectrum (XPS) of the Cs_2SnI_6 film; high-resolution XPS spectra and peaks fitting for: (b) Sn, (c) Cs, and (d) I 3d

The resistance increases with the introduction of NO_2 gas. The relationship between the device response and NO_2 concentration is shown in Fig. 7b. The sensitivity of the device to 3–20 ppm NO_2 exposure gas at room temperature for 5 min was determined as 8.30%, 11.73%, 20.98%, 26.81%, and 35.1%, respectively. The device response increases linearly with the NO_2 concentration (Fig. 7b). The correlation coefficient (R^2) is 0.998. The NO_2 detection limit of the sensor was measured as 3 ppm.

Reproducibility and long-term stability are also important parameters to evaluate the gas sensor performance. The response of Cs_2SnI_6 film toward 20 ppm NO_2 under six cycles for sensing testing at room temperature is shown in Fig. 7c. The device based on Cs_2SnI_6 exhibits good repeatability with a response of about 35%. Furthermore, as shown in Fig. 7d, the long-term stability of the Cs_2SnI_6 film was studied. The result shows the device response has a bit change after 25 days (from 35% to

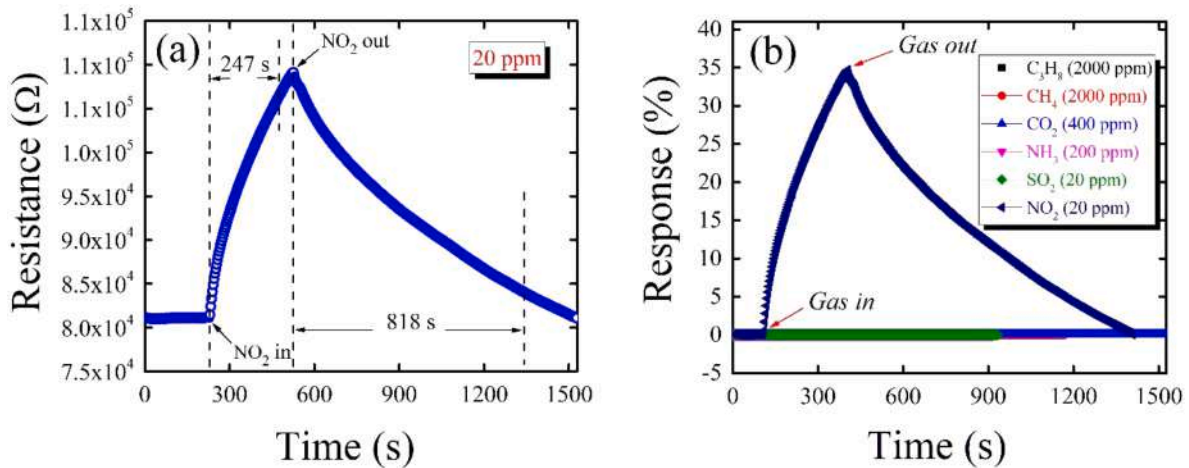


Fig. 6. Response/recovery curves of the Cs_2SnI_6 film based sensor at room temperature without light illumination exposed to (a) 20 ppm NO_2 and (b) several gasses.

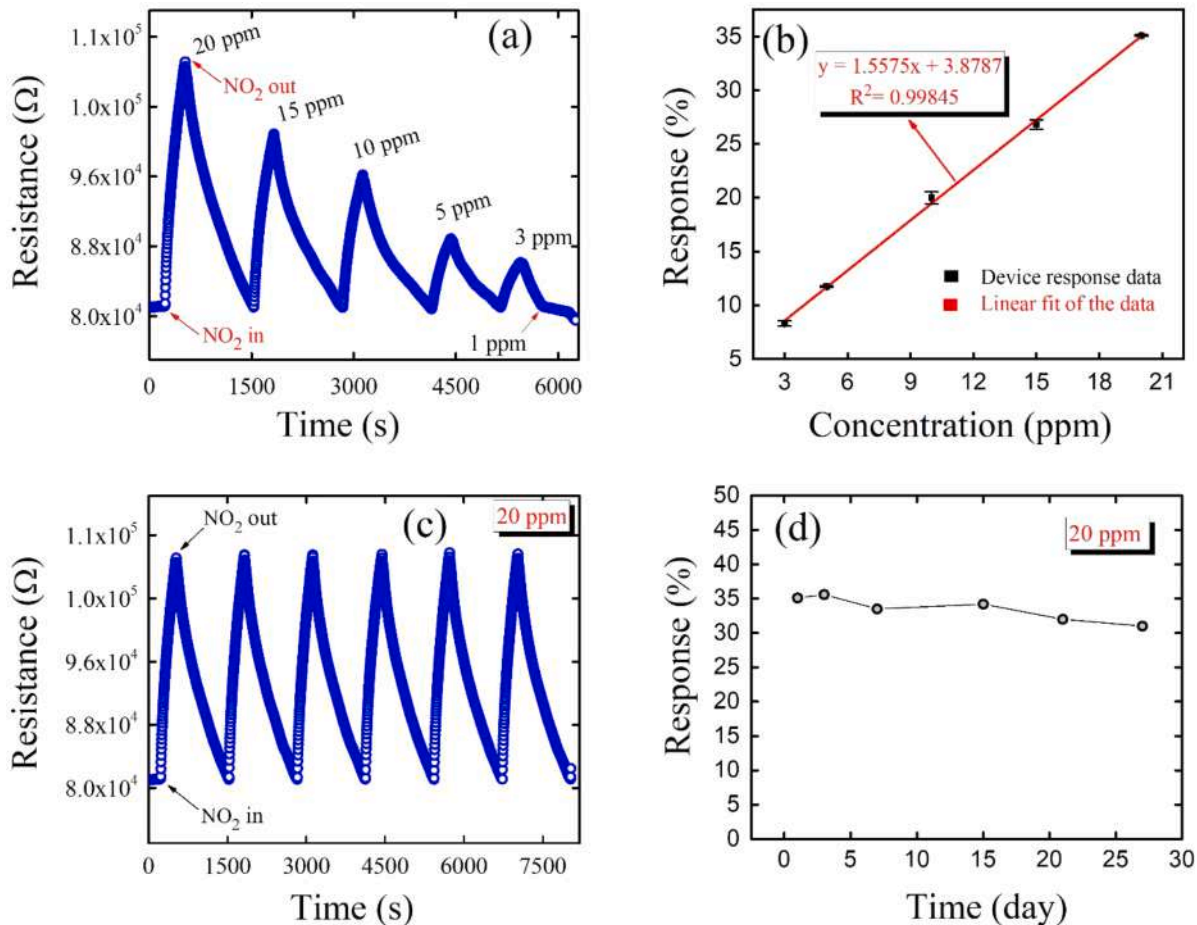


Fig. 7. Response of Cs_2SnI_6 film-based sensor at room temperature without light illumination: (a) Dynamic response of Cs_2SnI_6 film-based sensor upon exposure to NO_2 with various concentrations; (b) Relationship between the sensor response and NO_2 concentration; (c) Sensor repeatability to 20 ppm NO_2 for six cycles; (d) Long-term stability of the sensor to 20 ppm NO_2 .

~31%). This confirms the good long-term stability of the Cs_2SnI_6 film. Table 1 shows the comparison of room-temperature NO_2 sensing properties between Cs_2SnI_6 film in this work and previously reported. It is observed that the Cs_2SnI_6 device showed a good NO_2 performance without any light illumination [29–34].

The responses of as-synthesized Cs_2SnI_6 film under different relative humidity (RH) were tested as shown in Fig. 8. Fig. 8a shows the effect of

repeatedly exposing the sensor to 20 ppm NO_2 at RT under various RH atmospheres. The response is stable after the device is exposed to 200 ppm NO_2 for 2 sensing cycles. The base resistance of the device gradually decreases with the ambient humidity increasing, from 8.1×10^4 at 0% RH to 7.8×10^4 at 52% RH, and then rapidly drops to 2.1×10^4 at 75% RH. The reason for this is that physisorbed water induces an increase in conductivity via e^- injection due to the production of hydroxyl

Table 1

The comparison of Cs₂SnI₆ device with the reported sensors towards NO₂.

Material	Operating temp.	Concentration(ppm)	Sensitivity (%)	t _{res} /t _{rec} (s)	Detection range (ppm)	Ref.
DGaN	RT(28 °C)	100	19.00	>250/>600	10–100	[29]
rGO/SnO ₂	RT	100	2.80	300/300	1–100	[30]
Multilayer MoS ₂	RT	100	27.92	249/ unrecoverable	5–100	[31]
rGO/GaN Nanorods	RT(30 °C)	100	3.42	- / -	-	[32]
ZrGO fibers	RT	20	2.21	394/807	1.5–20	[33]
CNTs/SnO ₂	RT	100	1.80	600/1800	25–100	[34]
Graphene/ MAPbBr ₃	RT	1	~7.00	>900/>1800	0.25–1	[15]
Cs ₂ TeI ₆	Blue light at RT	1	4.36	125/600	0.025–1	[44]
Cs ₂ SnI ₆	RT(25 °C)	20	35.12	247/818	3–20	This study

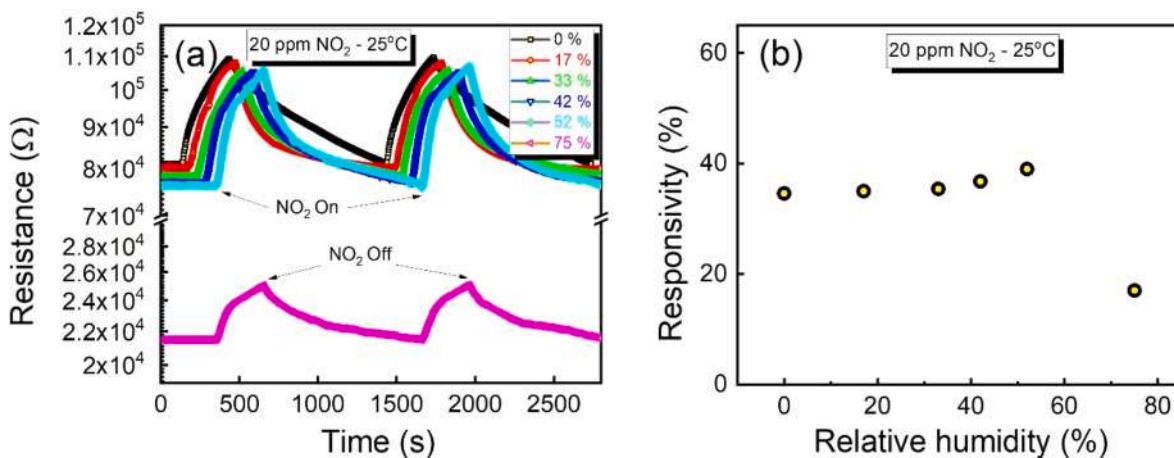


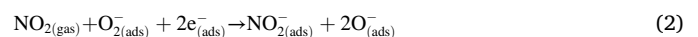
Fig. 8. (a) Effect of RH variation on the Cs₂SnI₆ film-based sensor to 20 ppm NO₂ at room temperature; (b) The relationship between the sensor response and RH toward 20 ppm NO₂ at room temperature.

radicals [35], which in turn reduces the device's resistance. The sensing response increases gradually negligible when the humidity increases from 0 to 52% RH and then rapidly drops to 17.03% at 75% RH (Fig. 8b). It is because the electron injection supplies more e^- (and O_2^- ion) on the surface of the Cs₂SnI₆ film at RH ambient conditions, following the enhancement of NO₂ response [36]. However, at high RH ($\geq 75\%$), the physisorbed water layer's covering covers the adsorption sites [35, 37, 38], resulting in a significant reduction in NO₂ reactivity, thus reducing responsivity of the device.

3.3. Gas sensing mechanism

The gas sensing mechanism of the Cs₂SnI₆-based sensor is similar to that of conventional n-type metal oxide semiconductor-based gas sensors: trapping electrons (charge carriers) in Cs₂SnI₆ film upon adsorbing target gas molecules. This mechanism is suitable for the gas sensing mechanism of several NO₂-sensitive materials at room temperature, such as CH₃NH₃PbI₃ [10], MASnI₃ [23]. A model of the Cs₂SnI₆ surface is proposed (Fig. 9) for explaining the NO₂ gas sensing mechanism of the sensor based on Cs₂SnI₆ film at room temperature. First, before exposure to NO₂ gas, dry air was introduced on the surface of the sensing element. The main defects in Cs₂SnI₆ material are iodine vacancies and tin interstitials [39]. Thus, when measured in air, oxygen tends to be adsorbed into these vacancies at the Cs₂SnI₆ surface, leading to the formation of $O_{2(ads)}^-$ ions at low temperatures (below 100 °C), presented: $O_{2(g)} \rightarrow O_{2(ads)}^-$; $O_{2(ads)}^- + e^- \rightarrow O_{2(ads)}^{2-}$ [40, 41]. The ionosorbed oxygen species capture electrons from the conduction band of Cs₂SnI₆ and form an electron-depletion layer (Fig. 9a). When the Cs₂SnI₆ film device is exposed to NO₂, NO₂ is capable of competitively capturing electrons not

only from the conduction band of the Cs₂SnI₆ film but also from chemisorbed oxygen species ($O_{2(ads)}^-$). These reactions may be given as follows [23, 42, 43]:



The formation of $NO_{2(ads)}^-$ and O^- from reactions 1, 2 could increase the thickness of the electron-depletion zones in the Cs₂SnI₆ film, resulting in the decrease the conductivity of the sensor film (Fig. 8b). One possibility is that when turning off NO₂ gas, $NO_{2(ads)}^-$ and O^- are desorbed at room temperature lead to increase in conductivity of the Cs₂SnI₆ film (Fig. 7c). This result is a big breakthrough for this kind of material-based gas sensor because of the difficulty of adsorbed NO₂ molecules' removal from the sensing material's surface at room temperature, without any aid from noble metal doping or light activity.

4. Conclusion

In summary, a 1- μ m-thick Cs₂SnI₆ film was successfully fabricated through a two-step process using a CVD system. FE-SEM studies revealed that the 360 nm diameter CsI spheres were synthesized in the first step, which was completely converted to Cs₂SnI₆ continuous film using SnI₄ vapor in the second step. The sensitivity and selectivity of the as-prepared Cs₂SnI₆ film-based device were measured at room temperature without light illumination with various target gases (C₃H₈, CH₄, CO₂, NH₃, SO₂, and NO₂). The sensor shows a similar behavior with the n-type semiconducting metal oxide. It can sensitively and selectively detect a 3 ppm limit of NO₂ gas. The sensor response to 20 ppm NO₂ was

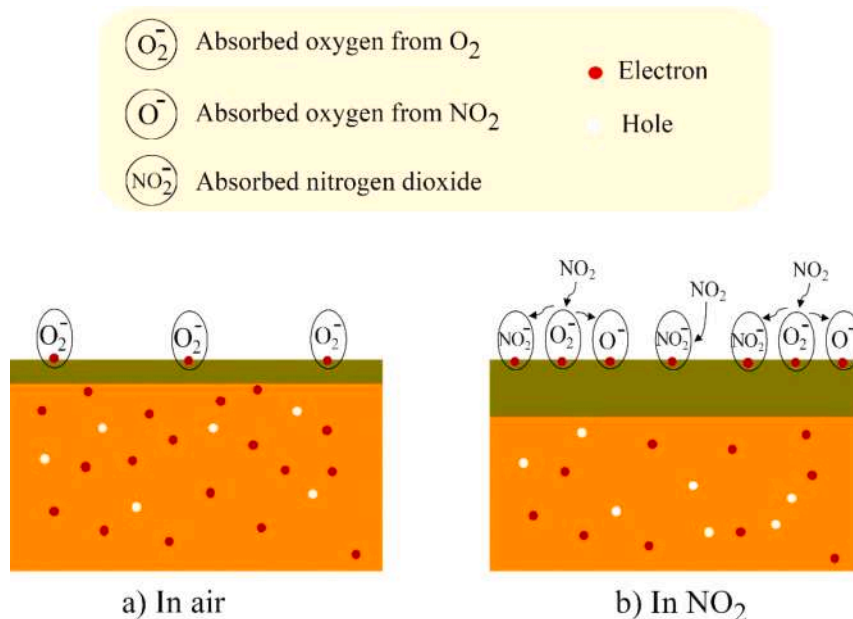


Fig. 9. Schematic diagram of NO_2 sensing mechanism of the Cs_2SnI_6 film.

determined to be nearly 35% under RH levels lower than 52%. This sensor can be operated at room temperature without any external source for recovery, indicating that the sensor based on Cs_2SnI_6 is a potential reliable application as a NO_2 gas sensor. In addition, this work provides knowledge on the gas sensing properties of Cs_2SnI_6 film and halide perovskites generally.

5. Author statement

I, corresponding author Young-Woo Heo, hereby confirm on behalf of myself and other authors, that this manuscript is our original work and has been neither published nor is being considered for publication elsewhere. All the authors have read and approved the manuscript and have agreed to the submission.

Declaration of Competing Interest

On behalf of all authors of the manuscript: “*Growth and NO_2 sensing properties of Cs_2SnI_6 thin film*”. I certify that there is no conflict of interest with any financial organization regarding the material discussed in the manuscript.

Acknowledgements

The work was supported by the National Research Foundation of Korea (NRF) grant funded by the Korea government (MSIP) [No. NRF-2020R1A4A2002161], and the grant from Le Quy Don Technical University.

Supplementary materials

Supplementary material associated with this article can be found, in the online version, at doi:10.1016/j.materresbull.2021.111628.

References

- [1] M. Lu, H. Wu, H. Wang, Y. HU, V.L. Colvin, Y. Zhang, W.W. Yu, *Chem Nano Mat* 5 (2019) 313–317.
- [2] C.F.J. Lau, Z. Wang, N. Sakai, J. Zheng, C.H. Liao, M. Gree, S. Huang, H.J. Snith, A. Ho-Baillie, *Adv. Energy Mater.* 9 (2019), 1901685.
- [3] H. Kim, J. Lee, H.R. Byun, S.H. Kim, H.M. Oh, S. Baik, M.S. Jeong, *Sci. Rep.* 9 (2019) 1–6.
- [4] H. Mehdi, A. Mhamdi, R. Hannachi, A. Bouazizi, *RSC Adv.*, 9 (2019) 12906–12912.
- [5] Y. Zhao, K. Zhu, *Chem Soc Rev* 45 (2016) 655–689.
- [6] J. Deng, J. Li, Z. Yang, M. Wang, *J. Mater. Chem. C* 7 (2019) 12415–12440.
- [7] Y. Zhuang, W. Yuan, L. Qian, S. Chen, G. Shi, *Phys. Chem. Chem. Phys.* 19 (2017) 12876–12881.
- [8] C. Bao, J. Yang, W. Zhu, X. Zhou, H. Gao, F. Li, G. Fu, T. Yu, Z. Zou, *Chem. Commun.* 51 (2015) 15426–15429.
- [9] M.-A. Stoeckel, M. Gobbi, S. Bonacchi, F. Liscio, L. Ferlauto, E. Orgiu, P. Samori, *Adv. Mater.* 29 (2017), 1702469.
- [10] X. Fu, S. Jiao, N. Dong, G. Lian, T. Zhao, S. Lv, Q. Wang, D. Cui, *RSC Adv.*, 8 (2018) 390–395.
- [11] M.Y. Zhu, L.X. Zhang, J. Yin, J.J. Chen, L.J. Bie, B.D. Fahlman, *Sens. Actuat. B Chem* 282 (2019) 659–664.
- [12] G. Kakavelakis, E. Gagaoudakis, K. Petridis, V. Petromichelaki, V. Binas, G. Kiriakidis, E. Kymakis, *ACS Sens.* 3 (2018) 135–142.
- [13] A. Maity, A.K. Raychaudhuri, B. Ghosh, *Sci. Rep.* 9 (2019) 1–10.
- [14] J.H. Kim, S.H. Kim, *Dye. Pigment.* 134 (2016) 198–202.
- [15] J. Casanova-Cháfer, R. García-Aboal, P. Atienzar, E. Llobet, *Sensors* 20 (2019) 4563.
- [16] J. Casanova-Chafer, R. Garcia-Aboal, P. Atienzar, E. Llobet, *Chem. Commun.* 63 (2020) 8956–8959.
- [17] S. Chatterjee, A.J. Pal, *J. Mater. Chem. A* 6 (2018) 3793–3823.
- [18] P.K.Singh Rahul, R. Singh, V. Singh, B. Bhattacharya, Z.H. Khan, *Mater. Res. Bull.* 97 (2018) 572–577.
- [19] F. Giustino, H.J. Snith, *ACS Energy Lett.* 1 (2016) 1233–1240.
- [20] T.C. Dang, H.C. Le, D.L. Pham, S.H. Nguyen, T.T.O. Nguyen, T.T. Nguyen, T. D. Nguyen, *J. Alloys Compd.* 805 (2019) 847–851.
- [21] X. Qiu, B. Cao, S. Yuan, X. Chen, Z. Qiu, Y. Jiang, Q. Ye, H. Wang, H. Zeng, J. Liu, M.G. Kanatzidis, *Sol. Energy Mater. Sol. Cells.* 159 (2017) 227–234.
- [22] Y. Chen, X. Zhang, Z. Liu, Z. Zeng, H. Zhao, X. Wang, J. Xu, *Microchim. Acta.* 186 (2019) 47.
- [23] V.X. Hien, P.T. Hung, J. Han, S. Lee, J.H. Lee, Y.W. Heo, *Scr. Mater.* 178 (2020) 108–113.
- [24] A. Kaltzoglou, M. Antoniadou, A.G. Kontos, C.C. Stoumpos, D. Pergati, E. Siranidi, V. Raptis, K. Trohidou, V. Psycharis, M.G. Kanatzidis, P. Falaras, *J. Phys. Chem. C* 120 (2016) 11777–11785.
- [25] B. Saparov, J.-P. Sun, W. Meng, Z. Xiao, H.-S. Duan, O. Gunawan, D. Shin, I. G. Hill, Y. Yan, D.B. Mitzi, *Chem. Mater.* 28 (2016) 2315–2322.
- [26] J. Zhang, S. Li, P. Yang, W. Liu, Y. Liao, *J. Mater. Sci.* 53 (2018) 4378–4386.
- [27] P.T. Hung, P.D. Hoat, V.X. Hien, H.-Y. Lee, S. Lee, Lee J-H, J.-J. Kim, Y.-W. Heo, *ACS Appl. Mater. Interfaces.* 12 (2020) 34274–34282.
- [28] X. Han, J. Liang, J.-H. Yang, K. Soni, Q. Fang, W. Wang, J. Zhang, S. Jia, A. A. Marti, Y. Zhao, J. Lou, *Small*, 15 (2019), 1901650.
- [29] M. Reddeppa, S.B. Mitta, B.-G. Park, S.-G. Kim, S.H. Park, M.-D. Kim, *Org. Electron.* 65 (2019) 334–340.
- [30] S. Mao, S. Cui, G. Lu, K. Yu, Z. Wen, J. Chen, *Mater. Chem.* 22 (2012) 11009–11013.
- [31] R. Kumar, N. Goel, M. Kumar, *ACS Sens.* 2 (2017) 1744–1752.
- [32] M. Reddeppa, B.-G. Park, M.-D. Kim, K.R. Peta, N.D. Chinh, D. Kim, S.-G. Kim, G. Murali, *Sens. Actuat. B Chem* 264 (2018) 353–362.
- [33] A.D. Ugale, G.G. Umarji, S.H. Jung, N.G. Deshpande, W. Lee, H.K. Cho, J.B. Yoo, *Sens. Actuat. B Chem* 308 (2020), 127690.
- [34] G. Lu, L.E. Ocola, J. Chen, *Adv. Mater.* 21 (2009) 2487–2491.

- [35] G. Rubasinghege, V.H. Grassian, *Chem. Commun.* 30 (2013) 3071–3094.
- [36] W. Yan, M.A. Worsley, T. Pham, A. Zettl, C. Carraro, R. Maboudian, *Appl. Surf. Sci.* 450 (2018) 372–379.
- [37] A. Mekki, G.D. Khattak, L.E. Wenger, *J. Non. Cryst. Solids* 31 (2006) 3326–3331.
- [38] N.M. Hung, N.M. Hieu, N.D. Chinh, T.T. Hien, N.D. Quang, S. Majumder, G.S. Choi, C. Kim, D. Kim, *Sens. Actuat. B Chem* 313 (2020), 128001.
- [39] Z. Xiao, Y. Zhou, H. Hosono, T. Kamiya, *Chem. Phys.* 17 (2015) 18900–18903.
- [40] A.S.M. Iftekhhar Uddin, D.T. Phan, G.S. Chung, *Sens. Actuat. B Chem* 207 (2015) 362–369.
- [41] P.T. Hung, V.X. Hien, P.D. Hoat, S. Lee, J.-H. Lee, J.-J. Kim, Y.-W. Heo, *Scr. Mater.* 172 (2019) 17–22.
- [42] M.B. Rahmani, S.H. Keshmiri, M. Shafiei, K. Latham, W. Wlodarski, J.D. Plessis, K. Kalantar-Zadeh, *Sens. Lett.* 7 (2009) 621–628.
- [43] C. Zhang, Y. Luo, J. Xu, M. Debliquy, *A: Physical* 289 (2019) 118–133.
- [44] P.D. Hoat, Y. Yun, B. Park, P.T. Hung, V.X. Hien, J.-H. Lee, S. Lee, Y.-W. Heo, *Scr. Mater.* 207 (2022), 114305.